



A *Trypanosoma brucei* ORFeome-Based Gain-of-Function Library Identifies Genes That Promote Survival during Melarsoprol Treatment

McKenzie Carter,^a Stephanie Gomez,^a Sam Gritz,^a Stephen Larson,^a  Eugenia Silva-Herzog,^b Hee-Sook Kim,^c Danae Schulz,^d  Galadriel Hovel-Miner^a

^aThe George Washington University, Department of Microbiology, Immunology, and Tropical Medicine, Washington, DC, USA

^bInstituto Nacional de Medicina Genómica, Mexico City, Mexico

^cThe Public Health Research Institute at the International Center for Public Health, New Jersey Medical School—Rutgers, The State University of New Jersey, Newark, New Jersey, USA

^dHarvey Mudd College, F.W.Olin Science Center, Claremont, California, USA

ABSTRACT *Trypanosoma brucei* is an early branching protozoan parasite that causes human and animal African trypanosomiasis. Forward genetics approaches are powerful tools for uncovering novel aspects of trypanosomatid biology, pathogenesis, and therapeutic approaches against trypanosomiasis. Here, we have generated a *T. brucei* cloned ORFeome consisting of >90% of the targeted 7,245 genes and used it to make an inducible gain-of-function parasite library broadly applicable to large-scale forward genetic screens. We conducted a proof-of-principle genetic screen to identify genes whose expression promotes survival in melarsoprol, a critical drug of last resort. The 57 genes identified as overrepresented in melarsoprol survivor populations included the gene encoding the rate-limiting enzyme for the biosynthesis of an established drug target (trypanothione), validating the tool. In addition, novel genes associated with gene expression, flagellum localization, and mitochondrion localization were identified, and a subset of those genes increased melarsoprol resistance upon overexpression in culture. These findings offer new insights into trypanosomatid basic biology, implications for drug targets, and direct or indirect drug resistance mechanisms. This study generated a *T. brucei* ORFeome and gain-of-function parasite library, demonstrated the library's usefulness in forward genetic screening, and identified novel aspects of melarsoprol resistance that will be the subject of future investigations. These powerful genetic tools can be used to broadly advance trypanosomatid research.

IMPORTANCE Trypanosomatid parasites threaten the health of more than 1 billion people worldwide. Because their genomes are highly diverged from those of well-established eukaryotes, conservation is not always useful in assigning gene functions. However, it is precisely among the trypanosomatid-specific genes that ideal therapeutic targets might be found. Forward genetics approaches are an effective way to identify novel gene functions. We used an ORFeome approach to clone a large percentage of *Trypanosoma brucei* genes and generate a gain-of-function parasite library. This library was used in a genetic screen to identify genes that promote resistance to the clinically significant yet highly toxic drug melarsoprol. Hits arising from the screen demonstrated the library's usefulness in identifying known pathways and uncovered novel aspects of resistance mediated by proteins localized to the flagellum and mitochondrion. The powerful new genetic tools generated herein are expected to promote advances in trypanosomatid biology and therapeutic development in the years to come.

KEYWORDS forward genetics, ORFeome, *Trypanosoma*, drug resistance mechanisms, parasitology, redox signaling

Citation Carter M, Gomez S, Gritz S, Larson S, Silva-Herzog E, Kim H-S, Schulz D, Hovel-Miner G. 2020. A *Trypanosoma brucei* ORFeome-based gain-of-function library identifies genes that promote survival during melarsoprol treatment. mSphere 5:e00769-20. <https://doi.org/10.1128/mSphere.00769-20>.

Editor Margaret Phillips, University of Texas Southwestern

Copyright © 2020 Carter et al. This is an open-access article distributed under the terms of the [Creative Commons Attribution 4.0 International license](https://creativecommons.org/licenses/by/4.0/).

Address correspondence to Hee-Sook Kim, heesook@rutgers.edu, Danae Schulz, dschulz@hmc.edu, or Galadriel Hovel-Miner, ghovel_miner@gwu.edu.

Received 28 July 2020

Accepted 21 September 2020

Published 7 October 2020

Trypanosomatids are a major parasitic lineage that include the African trypanosomes, American trypanosomes, and *Leishmania* spp. (family Trypanosomatidae, order Kinetoplastida), which collectively cause death and disease in millions of people living in tropical and subtropical regions (1). There are no vaccines against this family of parasites, and the limited number of antitrypanosomatid drugs present ongoing challenges of host toxicity, complex treatment regimens, and burgeoning drug resistance (2).

Trypanosomatid parasites appear to have diverged from a shared ancestor around 100 million years ago. These early branching eukaryotes have highly divergent genomes from those of well-established model organisms, with more than 35% of open reading frames (ORFs) annotated as hypothetical proteins (3). Of the 9,068 genes in the *Trypanosoma brucei* (African trypanosome) genome, 6,158 are orthologous with both *Trypanosoma cruzi* (American trypanosome) and *Leishmania major* (3). While reverse genetics based on well-established models can promote discrete advances, forward genetics approaches have the potential to uncover important aspects of trypanosomatid biology shared among orthologous genes.

T. brucei, the causative agent of human African trypanosomiasis (HAT), has historically been the most genetically tractable of the trypanosomatid parasites. For the past decade, a whole-genome RNA interference (RNAi) knockdown library has been the primary forward genetics tool in *T. brucei*, resulting in the identification of essential genes, genes associated with drug resistance and pathogenesis, and signaling factors critical to life cycle progression, to name a few (4–9). A strength of the RNAi library and associated RNA interference targeted sequencing (RIT-seq) approaches is the identification of genes that result in a loss-of-function phenotype (10). However, the RNAi library has some limitations. First, if the target of a genetic screen happens to be essential, it is difficult to identify using an RNAi screen. Second, while the RNAi library has been used to identify proteins involved in drug uptake (11) and activation (12), it cannot be used to identify the molecular target of drugs that selectively kill the parasite and not the host, since the molecular target is, by definition, essential in the parasite.

A gain-of-function library approach may be more effective in the identification of drug targets and resistance mechanisms (13–15). For example, overexpression of the molecular target can act as a sink, effectively mopping up the drug and promoting survival during drug treatment. This could be especially useful for identifying targets of inhibitors that are still in development (16) and has recently been used to identify a target of the antimalarial drug risdronate (17) and another antimalarial proteasome inhibitor (18). In basic biology, overexpression screens have been critical for discoveries in the areas of chromosome segregation, cell cycle, signal transduction, transcriptional regulation, cell polarity, and stem cell biology (19).

Traditional methods of overexpression library formation by cDNA synthesis and cloning are not viable for *T. brucei*, as most gene expression regulation in trypanosomatids occurs posttranscriptionally, with 5' and 3' untranslated regions (UTRs) playing a major role in determining steady-state levels of their associated transcripts (20). Existing *T. brucei* overexpression libraries generated by physical or enzymatic whole-genome fragmentation have generated useful results but lack the ability to ensure complete ORF integration and can include unwanted regulatory elements (21–24). In addition, random shotgun libraries can be used to identify a protein region required for a particular phenotype, but they are limited by the fact that partial proteins are not always folded properly and that the entire protein may be required for function, which can produce false positives and false negatives (25). In trypanosomatids, increased gene expression has been linked to drug resistance in *Leishmania* spp. through episomal cosmid amplification (25) and in *T. brucei* *in vitro* when enzymes of trypanothione biosynthesis are overexpressed (21, 26). ORFeome-based approaches, in which all ORFs in the genome are cloned for downstream applications, are powerful tools for the specific evaluation of gene effects whose proximal regulatory elements are excluded (27, 28). In addition, generation of an ORFeome can be applied to the downstream generation of multiple whole-genome methodologies, including yeast 2-hybrid librar-

ies, tagging libraries, and inducible expression libraries for gain-of-function studies (29–32).

In this study, we have taken an ORFeome-based approach to generate a *T. brucei* gain-of-function library for forward genetic screens. Melarsoprol was selected for a proof-of-principle genetic screen for its clinical significance, the probability that it affects multiple intracellular targets, and because its mode of cell killing is not completely understood (33, 34). Melarsoprol, an arsenical compound, has long been used for the treatment of second-stage (central nervous system) *T. brucei* infection (33). Second-stage HAT infections caused by *T. brucei* subsp. *gambiense* can now be treated by nifurtimox/eflornithine combination therapy (NECT) and the recently approved drug fexinidazole (2, 35). However, melarsoprol remains the only treatment for second-stage *T. brucei* subsp. *rhodesiense* infection, which rapidly progresses toward host death if left untreated. Melarsoprol treatment is burdened with high levels of host toxicity, challenging treatment regimens, and increasing reports of drug resistance and treatment failures (33). Melarsoprol is taken up into the cell by the P2 adenosine transporter (AT1) and aquaglyceroporin transporter (AQP2), which are mutated in most drug-resistant isolates (33). Redox metabolism in trypanosomatids is based predominantly on their unique dithiol molecule trypanothione and the trypanothione reductase (36). *In vivo*, melarsoprol is rapidly metabolized to trypanocidal metabolites including melarsen oxide, which binds trypanothione forming the stable adduct MeT (37); MeT is expected to have diverse effects on redox metabolism, ROS stress management, and the formation of deoxynucleoside triphosphates (dNTPs) by ribonucleotide reductase (33, 36). Despite the established relationship between melarsoprol and trypanothione, which aspect of trypanothione pathway inhibition results in parasite killing remains undetermined (33). Because the biosynthetic and redox utilization pathways contain enzymes unique to trypanosomatids, they have been broadly explored as drug targets against American trypanosomes and *Leishmania* species (20, 38–42).

Here, we present a description of the newly generated gain-of-function parasite library and describe its use in a screen for factors that increase parasite survival in the presence of melarsoprol. Library induction in the presence of melarsoprol resulted in the isolation of a specific survivor population consisting of 57 significantly overrepresented genes. Among these genes, we identified the gene encoding the rate-limiting enzyme of trypanothione biosynthesis (γ -glutamylcysteine synthetase, *Tb927.10.12370*), whose established relationship with melarsoprol validates the gain-of-function library's usefulness (26). In addition, we identified subsets of overrepresented genes encoding proteins associated with gene expression, the mitochondrion, and the flagellum whose association with melarsoprol had not been reported previously. Thus, the *T. brucei* ORFeome and resulting gain-of-function library that we generated are now positioned to provide new insights into trypanosomatid biology, pathogenesis, and drug resistance, which will promote the development of novel therapeutics.

RESULTS

Generation of a *Trypanosoma brucei* ORFeome. To generate a library consisting of all relevant ORFs from the *T. brucei* genome, start and stop sites for all *T. brucei* ORFs were obtained from available *TREU927* ribosomal profiling data for 9,200 genes (Fig. 1A) (43). We filtered out 1,956 ORFs unsuitable in size (<100 bp or >4,500 bp), coding for an undesired product (ribosomal genes, *VSGs*, *ESAGs*, pseudogenes), or annotated as “hypothetical unlikely.” Known multidrug-resistant channels (including MRPA, whose overexpression causes melarsoprol resistance) were also excluded (26). PCR primers for the resulting 7,245 targeted ORFs were designed *in silico* with *attB1* and *attB2* Gateway cloning sites with matched melting temperatures, synthesized, and resuspended in 21 separate 384-well plates that were organized by their anticipated ORF product size and gene annotations as either “known” or “hypothetical” (Table 1; also see Table S1 in the supplemental material for oligonucleotide sequences).

Each ORF was PCR amplified in 384-well format from Lister 427 genomic DNA. The general quality of the PCRs was assessed by the addition of SYBR green and measure-

A) *T. brucei* ORFeome Strategy

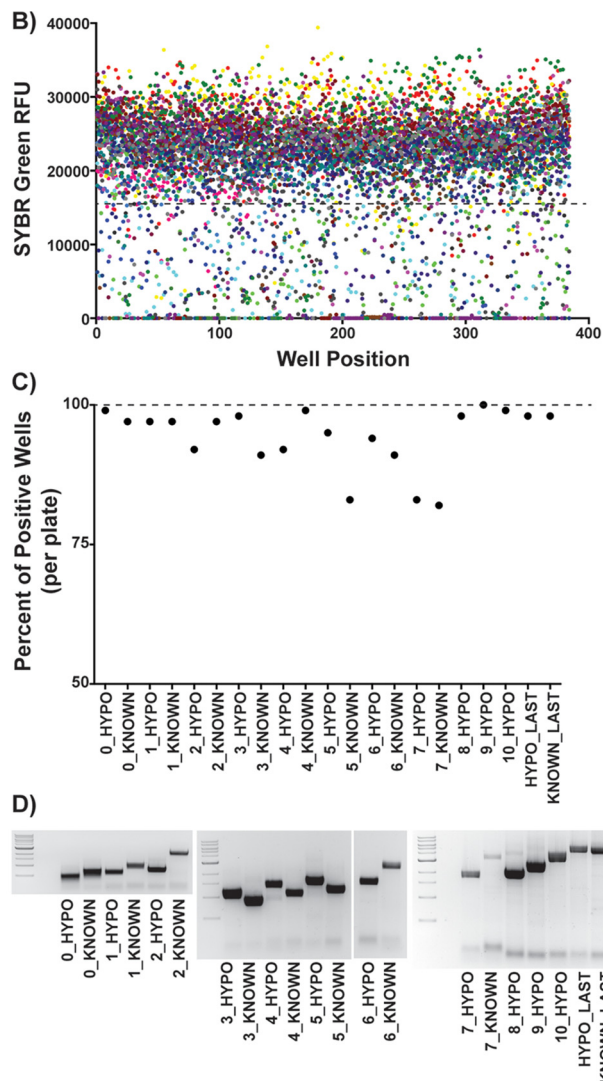
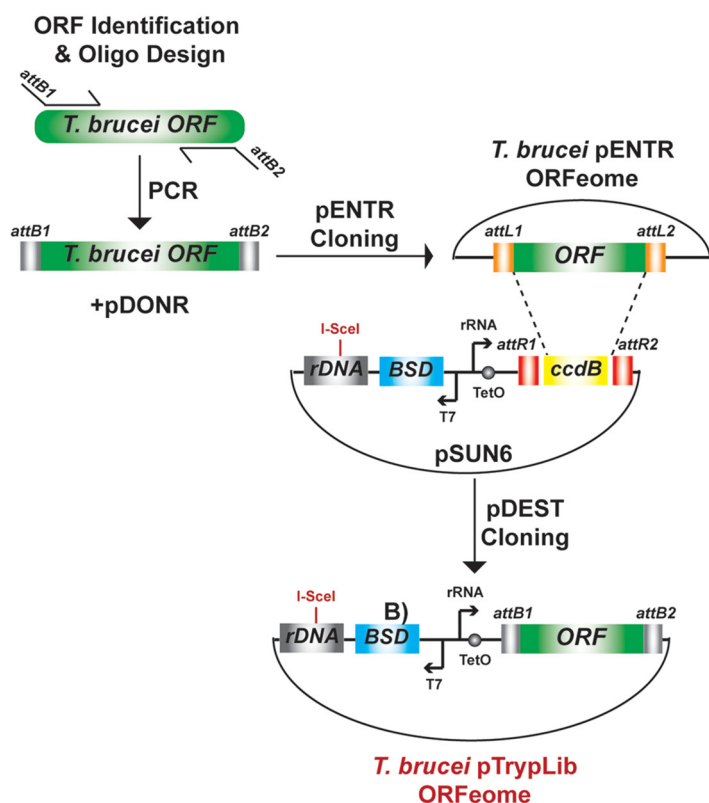


FIG 1 Generating a *T. brucei* ORFeome. (A) ORFeome cloning strategy: *attB* site addition to *T. brucei* ORFs during PCR amplification, BP Gateway cloning into pDONR221 to generate the pENTR ORFeome, and LR Gateway cloning into *T. brucei*-specific pDEST (pSUN6) (see Fig. S1 in the supplemental material) to generate the complete pTrypLib ORFeome. (B) Assessment of PCR amplification by SYBR green relative fluorescence units (RFU). Each color represents one of the 21 384-well plates, and each dot represents a PCR in a single well as measured by SYBR green RFU. (C) Percentages of PCR-positive wells (SYBR assessment) for each of the 21 384-well plates, from the first time amplified. (D) Agarose gel bands from each of the original 21 384-well PCR plates pooled prior to gel extraction and cloning, from the first time amplified, compared to 1-kb DNA ladder.

ment of the resulting relative fluorescence units (RFU) (Fig. 1B). Based on the SYBR green assessment, initial PCRs resulted in the successful amplification of 94% of the ORFeome (6,820/7,245 ORFs) (Fig. 1C). To increase ORFeome coverage, we reamplified 429 failed PCRs and succeeded in producing 228 products, resulting in a final total of 7,039 PCR products amplified (97.2% of the targeted genes).

PCRs from each 384-well plate were pooled (10 μ l from each well) into 21 corresponding PCR product pools, irrespective of the SYBR result, which maintained the product size range associated with each plate (Table 1). Each resulting size-sorted PCR pool was run on agarose gels and gel purified prior to Gateway cloning (Fig. 1D). Each size-sorted pool of gel-extracted PCR products was cloned into a standard pDONR Gateway cloning vector (pDONR221), as described (27, 44), to generate the pENTR ORFeome library. The resulting pENTR libraries were then transferred into a *T. brucei*-specific pDEST type vector with ribosomal DNA (rDNA) spacer targeting homology regions and a tetracycline-inducible system for ORF expression (Fig. 1A; see also Fig. S1). The resulting library of ORFs cloned for *T. brucei* genomic integration was termed the pTrypLib ORFeome.

TABLE 1 384-well oligo plates

Plate name	Min length (bp)	Max length (bp)	No. of ORFs per plate
0_hypothetical	102	375	373
0_known	147	591	315
1_hypothetical	375	522	374
1_known	594	849	365
2_hypothetical	522	666	372
2_known	849	1056	363
3_hypothetical	669	822	382
3_known	1056	1287	367
4_hypothetical	822	993	372
4_known	1287	1524	348
5_hypothetical	993	1155	365
5_known	1524	1857	342
6_hypothetical	1158	1365	375
6_known	1857	2337	362
7_hypothetical	1368	1635	378
7_known	2340	3504	376
8_hypothetical	1635	1953	381
9_hypothetical	1953	2508	381
10_hypothetical	2508	3501	381
hypothetical_last	3504	4488	135
known_last	3507	4497	138
Total			7245

Sequencing, assessment, and final coverage of the *T. brucei* ORFeome. The *T. brucei* pENTR and pTrypLib ORFeome-harboring plasmids were each pooled and prepared for Illumina sequencing by tagmentation, in which a modified transposition reaction is used to cleave DNA and insert adaptors for high-throughput sequencing (45). To assess which of the 7,245 targeted ORFs were not present in the pENTR and pTrypLib ORFeomes, we aligned the sequencing reads to the *TREU927* genome, removed PCR duplicates, and counted the number of reads corresponding to each targeted ORF. Because we knew that some of the targeted genes were highly similar or duplicated, we aligned the reads under two modes, one that required unique alignments and one that allowed multiple alignments. Both data sets were then assessed to determine how many genes were “missing” from each library, defined as any targeted gene with zero aligned reads.

Initial analysis showed 1,845 missing ORFs from the pENTR library and 2,593 missing ORFs from pTrypLib (Fig. 2A, pENTR_1, pTrypLib_1, unique alignments). To increase the number of ORFs in the final library, PCR products corresponding to each missing ORF were isolated from the original PCR plates. The resulting eight additional size-sorted ORF pools were gel purified, Gateway cloned (see Table S2 for cloning pools including “MISS_1-8”), sequenced by tagmentation, and analyzed as described above. The final ORFeomes were missing 457 ORFs from the pENTR library and 636 ORFs from pTrypLib (Fig. 2A, pENTR_Final, pTrypLib_Final, uniquely aligned reads, and see Data Set S1 for tables of all genes present). The final pTrypLib ORFeome contains 6,609 uniquely aligned and 6,803 multiply aligned *T. brucei* ORFs, resulting in 91% to 94% inclusion of the targeted ORFeome.

To analyze whether large or small genes were overrepresented in the set of missing genes (unsuccessfully cloned ORFs), we compared the distributions of gene lengths between the target set of ORFs (Fig. 2B, red bars) and missing genes (Fig. 2B, blue and teal bars). The distributions of gene lengths were similar, indicating that cloning failure was likely independent of gene size.

Coverage of each ORF in pTrypLib was analyzed by count distribution based on the number of reads aligned. Most ORFs resulted in \log_2 reads per kilobase per million (RPKM) values between 0 and 10 (Fig. 2C and Fig. S2, top right). Thus, the numbers of poorly represented ORFs (RPKM < 1) were 195 for uniquely aligned reads and 369 for

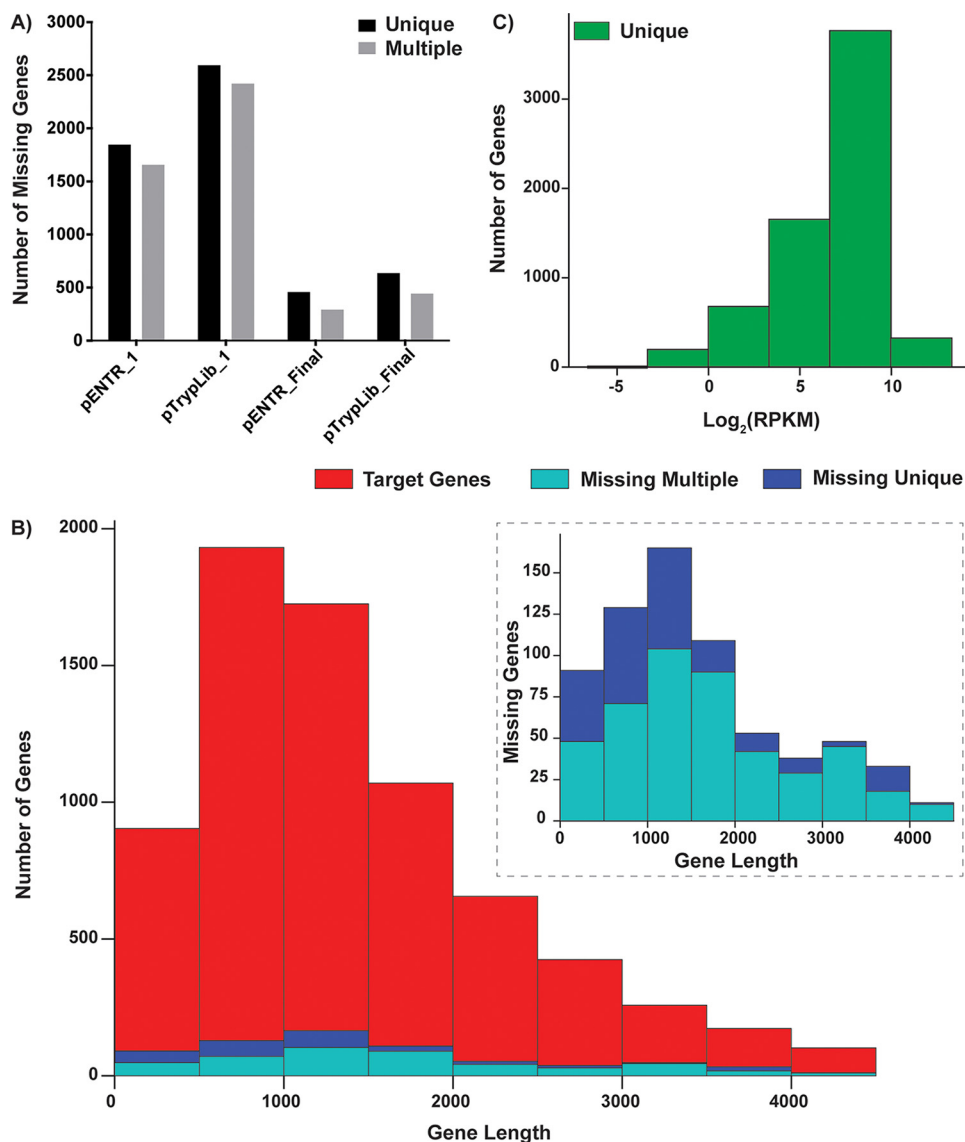


FIG 2 Assessment of pENTR and pTrypLib plasmid libraries. (A) Bar graph showing the number of targeted ORFs with zero detectable aligned reads from the first round of cloning (pENTR_1 and pTrypLib_1) and after both rounds of cloning (pENTR_Final and pTrypLib_Final) using analyses generated from both uniquely and multiply aligned reads. (B) Histograms showing the distribution of ORF lengths for the target gene list (red) and the set of ORFs with zero detectable aligned reads after both rounds of cloning (labeled as missing). Analyses from unique (dark blue) and multiply (light blue) aligned reads are shown. (Inset graph) Target ORF lengths have been left out to better visualize the lengths of the missing ORFs. (C) Histogram showing the distribution of normalized read counts for each ORF in the pooled pTrypLib plasmid libraries (uniquely aligned reads shown) (see Fig. S2 for both uniquely and multiply aligned reads).

multiply aligned reads, representing 3% and 5% of all ORFs in the library, respectively. We then determined if ORF length affected representation in the library by plotting the \log_2 RPKM value against ORF length (Fig. S2). No strong correlation was observed between ORF length and coverage in the pTrypLib ORFeome, with a best fit line showing a small negative slope for both unique and multiply aligned reads (-0.00067 and -0.00077 , respectively). Thus, in general, shorter ORFs are not significantly more highly represented than longer ORFs (Fig. S2).

A *T. brucei* gain-of-function parasite library. The pTrypLib ORFeome contains more than 6,500 tetracycline-inducible ORFs ready for *T. brucei* genomic integration at an rDNA spacer site. The landing pad (LP) system, developed for RIT-Seq library screens, was employed to ensure faithful integration into a single rDNA spacer site and high

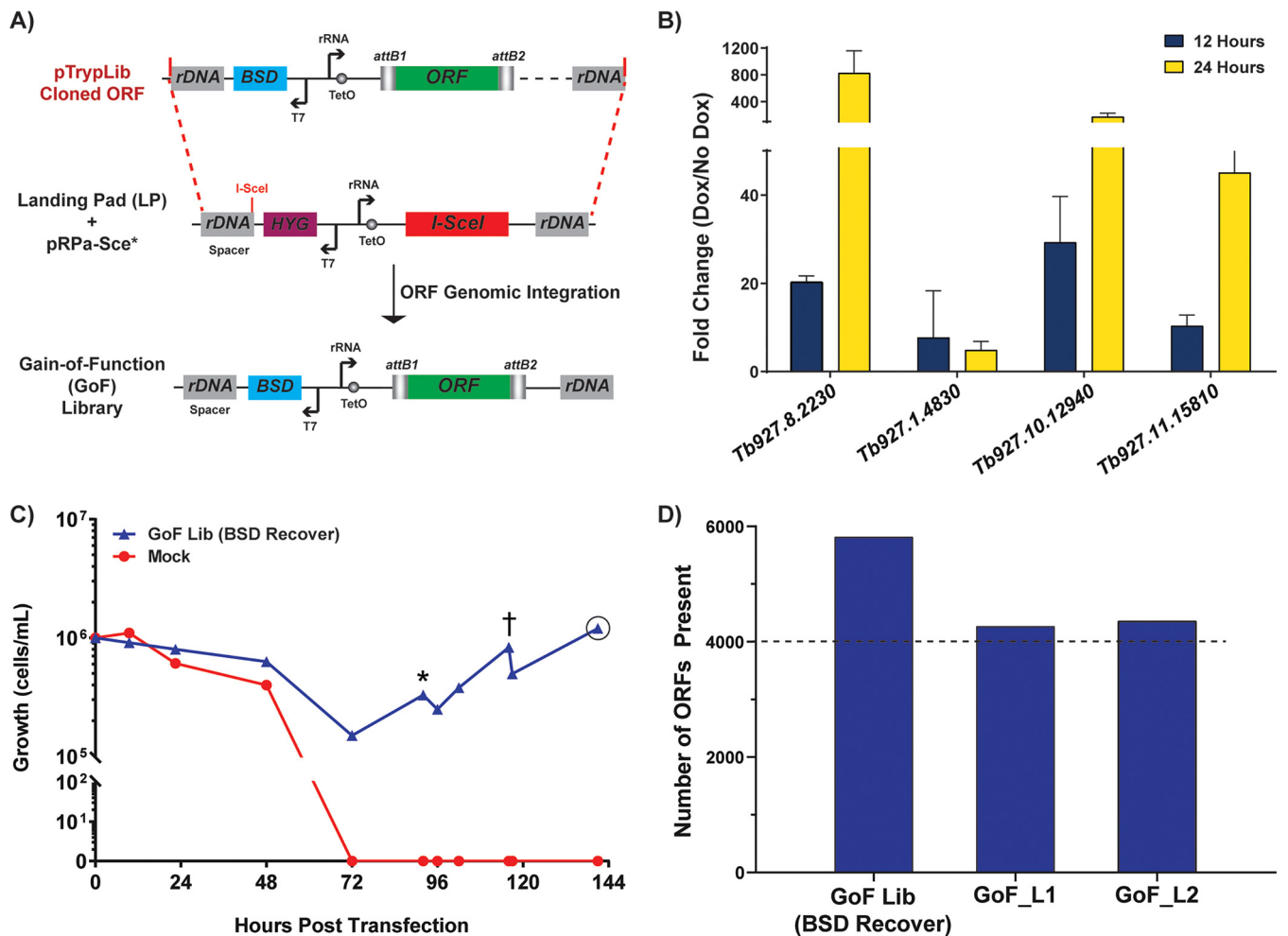


FIG 3 Generation and validation of the *T. brucei* GoF library. (A) Transfection of pTrypLib ORFeome into parental landing pad (LP) cell line harboring pRPaSce* plasmid for I-SceI-induced enzymatic cleavage of a single rDNA spacer site to increase transfection efficiency, as previously reported (6). (B) Inducible expression of a low-complexity GoF library measured by RT-qPCR following 12 and 24 h of doxycycline induction compared to that in uninduced cells (no Dox). (C) Generation of the pTrypLib ORFeome-based GoF parasite library. Graph shows the recovery of GoF library-harboring cells (blue line) compared to that from mock transfection (red line) in blasticidin (BSD) (“BSD recover” indicates recovery of the selected GoF library) added at time 0, 12 h posttransfection. *, cells spun and resuspended in 300 ml HMI-9; †, addition of 500 ml HMI-9; ○, time of GoF library harvest. (D) Assessment of the number of ORFeome genes present in the GoF library following initial transfection [GoF Lib (BSD recover), blasticidin-recovered population] and following freeze-thaw and 3 days of growth to generate GoF_L, which was then used to generate NGS libraries using two alternative protocols (see Materials and Methods) resulting in GoF_L1 and GoF_L2.

transfection efficiency (Fig. 3A), which is promoted by the site-specific induction of an I-SceI DNA break, as described previously (6).

Prior to transfection of the full pTrypLib ORFeome, we sought to verify inducible expression of this system using a low-complexity library. The low-complexity library was generated by transfecting a small number of equimolar pooled ORFs and recovering a single population of parasites. Thus, we generated an ORF library with 1,000 times less complexity than the complete pTrypLib. The low-complexity library was then grown with or without doxycycline (Dox) induction for 12 or 24 h prior to RNA extraction and reverse transcription-quantitative PCR (RT-qPCR) analysis to measure inducible expression of the transfected ORFs. ORFs showed increased transcript levels following Dox induction at 12 and 24 h; 3 of the 4 ORFs analyzed resulted in approximately 10- to 30-fold increased transcript levels after 12 h and 50- to 600-fold increases in transcript levels after 24 h (Fig. 3B). Thus, the overall strategy of ORFeome exogenous transcription induction from pTrypLib cloned ORFs was deemed viable.

The full pTrypLib ORFeome was then used to generate an inducible *T. brucei* gain-of-function (GoF) library by transfecting 360 million LP cells and selecting with

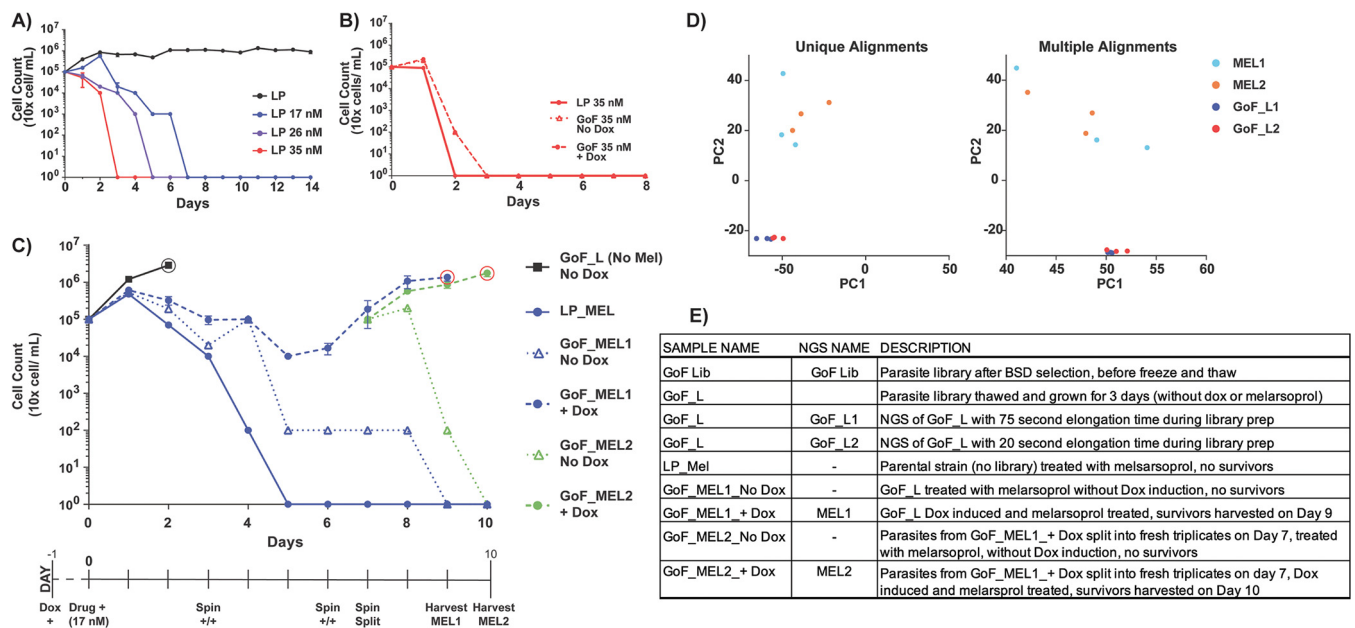


FIG 4 Isolation of melarsoprol survivor populations from a GoF screen. (A) Growth of landing pad (LP) parental cell line in 17 nM (blue line), 26 nM (purple line), 35 nM (red line), or no (black line) melarsoprol (black line). (B) GoF library screen in 35 nM melarsoprol treatment: LP cell line, solid red line; uninduced GoF library, red dotted line; induced GoF library, red dashed line. Dotted and dashed lines overlap. (C) GoF genetic screen in 17 nM melarsoprol. Timeline at the bottom of the graph indicates days on which either Dox (+Dox), melarsoprol (+Drug), or both (+/+) were added. All cultures (other than GoF_L) were continuously grown in the presence of 17 nM melarsoprol. On days 3, 6, and 7, the triplicate cultures were centrifuged and resuspended in fresh medium with melarsoprol and Dox for induction (noted as spin +/+). Biological triplicate cultures are as follows: GoF_L, untreated GoF library-harboring cells grown for 3 days (black line); LP parental cell line, solid blue line; uninduced GoF library (no Dox), blue triangles on dotted line; induced GoF library (+ Dox), blue circles on dashed line, harvested on day 9 (red circle on blue line) to produce MEL1. On day 7, biological triplicates from GoF_MEL1 +Dox (blue circles on dashed line) were split into two sets of triplicate samples, both in 17 nM melarsoprol, one of which was not further induced (no Dox, green triangles on dotted line). The other continued to be induced (+Dox, green squares on dashed green line) and was harvested on day 10 to produce MEL2 (red circle indicates harvest). (D) Principal-component analysis (PCA) comparing GoF_L libraries (L1 and L2) (see Materials and Methods) with libraries arising following continuous melarsoprol selection (MEL1 and MEL2). (E) Table of sample names and NGS sequencing samples with full description.

blasticidin (BSD) (6). Sixty million cells survived transfection, which were then propagated to 3 billion cells over 3 days to generate the *T. brucei* GoF library (Fig. 3C, blue line). Illumina sequencing libraries were prepared using a custom P5 forward oligonucleotide containing *attB1* site complementarity and a universal P7 reverse oligonucleotide. Indexed products were Illumina sequenced using a custom oligonucleotide complementary to the *attB1* site upstream of the introduced ORF. Thus, the resulting sequencing reads primarily correspond to the 5' ends of the introduced ORF (see Fig. S3). Immediately following transfection and recovery in blasticidin, the *T. brucei* GoF library consisted of 5,819 ORFs [Fig. 3D, GoF Lib (BSD recover)] and then approximately 4,300 ORFs following freeze thaw (Fig. 3D, GoF_L1 and GoF_L2) (alternative sequencing conditions described in Materials and Methods). It is unclear if the apparent loss of approximately 1,500 ORFs arose through an artifact associated with a relatively low number of next-generation sequencing (NGS) reads returned from those samples or a true loss of content between library transfection and the subsequent thawing of frozen library.

Isolation of melarsoprol survivors by gain-of-function genetic screening. To identify ORFs whose induced expression promoted survival in the presence of lethal doses of melarsoprol, we tested three concentrations of drug on the LP cell line. Similar to previous reports, we observed that *T. brucei* LP cells died after 3 days in 35 nM, 5 days in 26 nM, and 7 days in 17 nM melarsoprol (17 nM is approximately two times the standard 50% effective concentration [EC₅₀] in culture and significantly less than concentrations used in clinical treatments) (Fig. 4A) (10). In a GoF genetic screen using 35 nM melarsoprol, no survivor population emerged (Fig. 4B, red dashed and dotted lines overlap). Thus, 17 nM melarsoprol was selected for a GoF genetic screen to allow more time for induced ORF expression that might confer resistance.

A GoF survivor screen was conducted in 17 nM melarsoprol for 10 days. As a control, GoF library-harboring parasites were grown in triplicate for 3 days (day –1 through day 2) without melarsoprol or Dox treatment to generate NGS libraries representative of all ORFs present prior to selection [Fig. 4C, GoF_L (no Mel), harvested on day 2, black circle). All other cultures were under continuous 17 nM melarsoprol (Mel) selection in triplicate for the following conditions: (i) landing pad (LP_MEL), (ii) GoF library parasites without Dox induction (GoF_MEL1 no Dox), and (iii) GoF library parasites with Dox induction (GoF_MEL1 +Dox). The timeline at the bottom of Fig. 4C shows when Dox was added, when melarsoprol [“drug (17 nM)”] was added, and when cells were spun and resuspended in fresh medium (“spin”), which was always replenished with the appropriate treatment (Dox/drug [+/+]).

Following 4 days of melarsoprol treatment, LP had cell counts below the limit of detection (10,000 cells/ml) and, from day 5 on, showed no signs of life (Fig. 4C, LP_MEL, solid blue line). On day 5, uninduced GoF library counts were below the limit of detection (Fig. 4C, GoF_MEL1 no Dox, dotted blue line), whereas induced GoF library resulted in a survivor population (Fig. 4C, GoF_MEL1 +Dox, dashed blue line). While a survivor population did not arise from uninduced GoF Library, parasite death was delayed by at least 1 day compared with that for LP (Fig. 4C, dotted blue line). Persistence of uninduced GoF library parasites in the presence of melarsoprol is probably the result of leaky gene expression from the rDNA spacer, an established caveat of this approach (46). The population of melarsoprol survivors arising from the induced GoF library (GoF_MEL1 +Dox) began to replicate efficiently in the presence of drug following day 5. On day 7, the triplicate samples were split into an additional 3 flasks that did not receive Dox induction (GoF_MEL2 no Dox, green dotted line) and 3 with Dox added (GoF_MEL2 +Dox, green dashed line); all continued to undergo 17 nM melarsoprol treatment. Only Dox-induced GoF library cultures were able to grow in the presence of melarsoprol (Fig. 4C, blue and green dashed lines), suggesting that library induction promoted survival in these populations.

The resulting Dox-induced populations of survivors, termed GoF_MEL1 (MEL1) and GoF_MEL2 (MEL2) (Fig. 4E summarizes sample nomenclature), were harvested for genomic DNA extraction at days 9 and day 10, respectively (Fig. 4C, red circles). Genomic DNAs from biological triplicate cultures of GoF_L (no melarsoprol treatment), MEL1 (initial population of survivors), and MEL2 (secondary population of survivors) (9 cultures total grown to ~1 million cells per ml, 200 ml each) were prepared for NGS analysis. The genomic DNA (gDNA) arising from GoF_L was prepared for NGS analysis using two elongations times to determine if this parameter biased the results, generating GoF_L1 and GoF_L2 (described in Materials and Methods).

We performed principal-component analysis (PCA) on the resulting sequencing data using both unique and multiple alignments (Fig. 4D). The PCA analysis shows two clearly separated clusters for untreated and melarsoprol-treated samples, with most biological replicates clustering together. DNAs arising from melarsoprol survivor populations (MEL1 and MEL2) were distinct from those of untreated GoF_L and showed more variation between samples (Fig. 4D, GoF_L1 and GoF_L2 versus MEL1 and MEL2). We observed, at best, a weak negative association between gene length and normalized read count (slopes of –0.00042 and –0.00045 for unique and multiple alignment analyses, respectively), indicating that ORF representation in the library is largely independent of ORF length (see Fig. S4)

Identification of overrepresented gain-of-function ORFs in melarsoprol survivors. We reasoned that any gene whose induction contributed to melarsoprol resistance should be overrepresented in induced libraries generated from melarsoprol survivor populations. To determine the fold change that represents a valid difference between melarsoprol-treated and untreated conditions, we compared each of the three biological replicates of GoF_L2 to one another and counted the number of ORFs with a 1.5-, 2.0-, or 4.0-fold change in normalized read count (Fig. 5A). By evaluating the biological variation between similarly treated replicates, we found that while many ORFs varied in normalized read count by greater than 1.5-fold between replicates (more

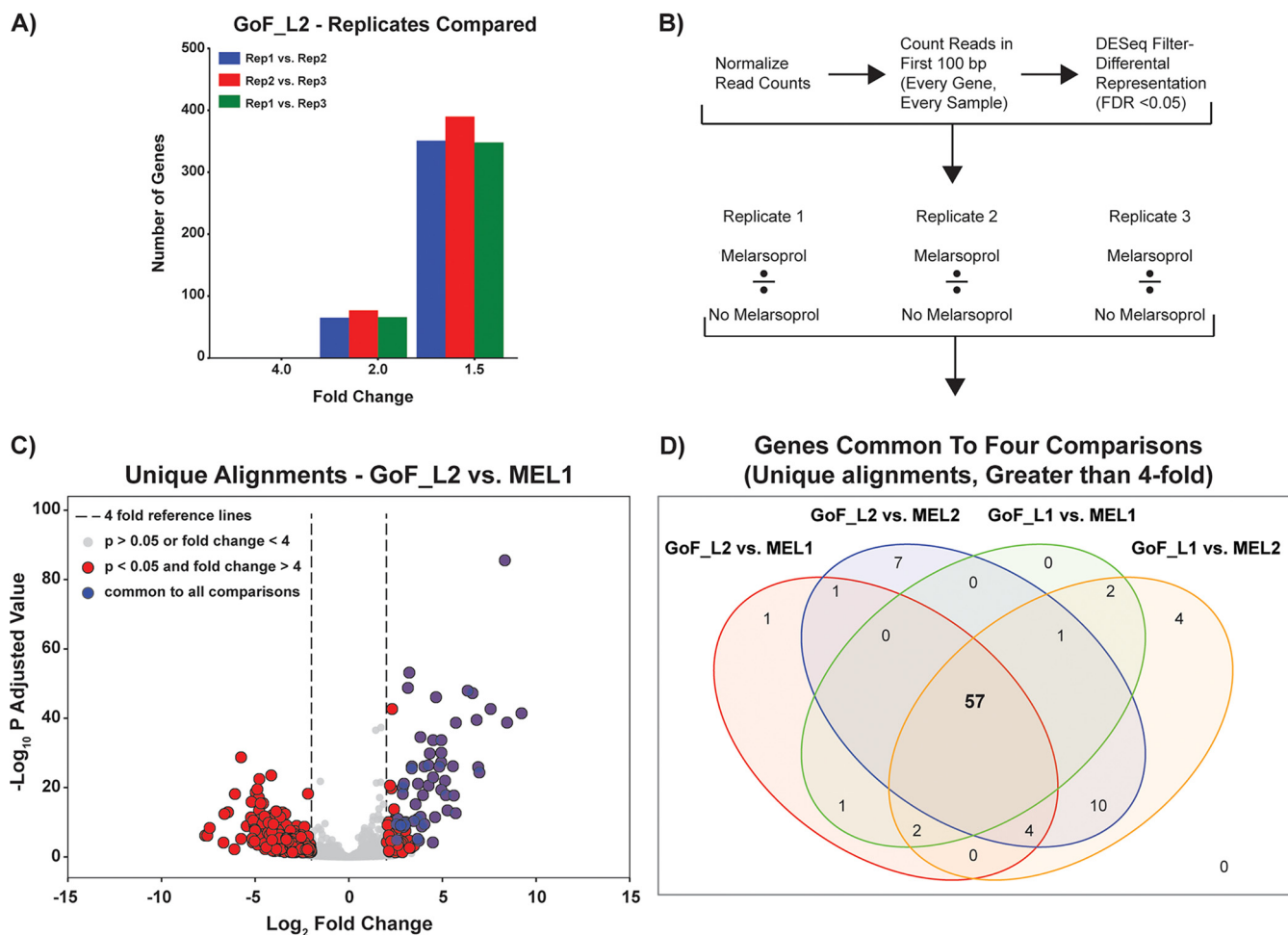


FIG 5 Identification of significantly overrepresented ORFs in melarsoprol GoF survivor populations. (A) The numbers of genes with changes of >1.5 -, 2 -, or 4 -fold for comparisons among all three replicates (Rep1, Rep2, and Rep3) of GoF_L2. (B) Hit-calling pipeline to identify genes overrepresented in melarsoprol survivor populations. (C) Volcano plot showing the $-\log_{10} P$ adjusted values versus \log_2 fold change in normalized counts for the comparison of melarsoprol-selected MEL1/GoF_L2 for each ORF in the targeted library. Blue dots represent overrepresented ORFs common to all four comparisons described in panel D. (D) Venn diagram illustrates the significantly overrepresented genes common to each comparison between GoF_L (GoF_L1 and GoF_L2) and melarsoprol treated (MEL1 and MEL2) and shared among all comparisons between replicates, resulting in 57 overrepresented hits identified in melarsoprol survivor populations compared to those in GoF_L populations.

than 300), very few ORFs varied by greater than 4-fold (Fig. 5A) (similar results obtained from GoF_L1, data not shown). Thus, we used a 4-fold change in normalized read count between melarsoprol-treated and untreated samples as the minimum threshold for identifying an ORF as overrepresented (a “hit”) in this study.

To identify ORFs that were overrepresented in the melarsoprol-selected population, we analyzed the aligned reads using DESeq2 and selected genes that were ≥ 4 -fold overrepresented with an adjusted P value of less than 0.05 (Fig. 5B). We used reads exclusively within the first 100 bp of each ORF (Fig. S3B). Four different comparisons were analyzed using this pipeline: GoF_L1 versus MEL1, GoF_L1 versus MEL2, GoF_L2 versus MEL1, and GoF_L2 versus MEL2 (Fig. 5B; see also Data Set S2 for raw and DESeq2 normalized reads). Figure 5C shows a volcano plot of DESeq2-generated significance values versus fold change for the comparison between GoF_L2 and MEL1. After hits had been called for each individual comparison, we identified the hits common among all 4 comparisons for both uniquely and multiply aligned reads (Fig. 5D; see also Data Set S3 for tables of all comparisons). These analyses resulted in the identification of 57 overrepresented ORFs (uniquely aligned) in the GoF melarsoprol survivor populations compared to those in GoF_L populations. In the comparison of GoF_L2 versus MEL1 depicted in the volcano plot, we observe that these 57 ORFs common to all the

comparisons were among the most highly overrepresented genes and with some of the lowest *P* adjusted values determined by DESeq2 (Fig. 5C, blue dots). Similar results were obtained for all comparisons between melarsoprol-selected and untreated GoF_L samples. An important caveat is that genes whose overexpression confers a significant survival advantage could very well show up as false positives within the set of genes identified to promote survival in melarsoprol. This is further explored in the Discussion section.

Melarsoprol resistance resulting from GoF hit overexpression. The 57 genes overrepresented in melarsoprol survivor populations are predominantly annotated as conserved hypothetical proteins or have putative functional assignments. To categorize all 57 genes, we utilized microscopic and proteomic localization data (47) (curated through TriTrypDB) and available publications (listed in Table 2) that addressed protein functionality. Based on this analysis, we organized the hits into specific categories and found that the top three groups were associated with gene expression (16 genes), the mitochondrion (10 genes), and the flagellum (10 genes) (Table 2). The gene expression category was further divided into those associated with splicing (5 genes), posttranscriptional regulation (5 genes), and translation (3 genes). It is important to note that categories based on localization were predominantly derived from data generated in insect stage (procyclic form) parasites, though some can also be confirmed from specific bloodstream-form data (47–49). Based on these categories and the fold overrepresentation of each ORF in melarsoprol survivors, we selected a subset of genes to analyze their effects on melarsoprol resistance.

We cloned a subset of overrepresented genes into a standard overexpression vector, transfected bloodstream-form *T. brucei*, and analyzed the effect of overexpression on melarsoprol resistance in cell viability assays (Fig. 6). The essential gene encoding γ -glutamylcysteine synthetase (GSH1; *Tb927.10.12370*) (50), which is the rate-limiting step of trypanothione biosynthesis (26, 38, 42, 51), was 191-fold overrepresented in melarsoprol survivors (Table 2). Trypanothione is the primary intracellular target of melarsoprol, and overexpression of GSH1 in *T. brucei* and other trypanosomatids increases the concentration of intracellular trypanothione, resulting in melarsoprol resistance under laboratory conditions (52). In our hands, overexpression of GSH1 resulted in an approximately 1.5-fold increase in the relative EC₅₀ of melarsoprol (Fig. 6A and E). The occurrence of GSH1 among the most overrepresented melarsoprol GoF survivors supports the usefulness of this tool in identifying drug targets.

We then evaluated the overexpression of three genes not previously linked to melarsoprol resistance, which were categorized as mitochondrial (*Tb927.11.590*, 350-fold overrepresented), gene expression (*Tb927.7.2780*, 322-fold overrepresented), and flagellar (*Tb927.9.15020*, 31-fold overrepresented). The most pronounced effect was a 2-fold increase in relative EC₅₀ of melarsoprol following the overexpression of *Tb927.7.2780*, which encodes the putative posttranscriptional activator XAC1 (expression activator 1) (Fig. 6C and E) (24). Overexpression of the mitochondrion-localized protein encoded by *Tb927.11.590* resulted in a >1.5-fold shift in the relative EC₅₀ of melarsoprol. Similarly, overexpression of the flagellar protein encoded by *Tb927.9.15020* resulted in an approximately 1.5-fold increase relative EC₅₀ of melarsoprol (Fig. 6D and E). Together, these results show that genes identified in melarsoprol GoF screening can promote drug resistance upon overexpression. Our results further support trypanothione as a major target of intracellular melarsoprol and implicate novel genes and mechanisms of melarsoprol resistance in trypanosomatids.

DISCUSSION

The forward genetics tools generated here address an urgent need to extend genomic functional characterization in *T. brucei* and its trypanosomatid relatives. More than 30 years of genetic and biochemical studies in trypanosomatids, 10 of which included the extensive use of an RNAi-based loss-of-function library, have produced key discoveries in parasitology and basic biology (53). Yet, with the functions of more than

TABLE 2 Hits overrepresented in melarsoprol survivors (comparison of GoF_L2 vs. MEL1)^a

Gene ID	Description (TrypTag 062920)	Localization (TrypTag or proteome)	PubMed	Category	Fold change overrepresented	DESeq P-adjusted value
Tb927.4.4810	Hypothetical protein, conserved	Cytoplasm (points, weak), endocytic		Endocytic +	597	3.77E-42
Tb927.1.1590	Hypothetical protein, conserved	Strong mitochondrial signal		Mitochondrial*	350	1.81E-39
Tb927.7.2780	Hypothetical protein, conserved, XAC1	Cytoplasm	26784394	Gene Expression#	322	2.83E-86
Tb927.10.12370	Gamma-glutamylcysteine synthetase, GSH1	Nucleoplasm	8663359	Biosynthetic#	191	2.19E-43
Tb927.5.3450	Eukaryotic translation initiation factor eIF2A ^Δ	Strong cytoplasm signal	24945722	Gene Expression#	126	4.50E-25
Tb927.1.11435	Dynein light chain lc6	Strong flagellum axoneme signal		Flagellar +	120	1.30E-26
Tb927.7.6190	Ring finger domain containing protein, ubiquitin ligase ^Δ	Strong endocytic system signal		Endocytic +	113	3.13E-40
Tb927.1.12380	Hypothetical protein, conserved	Nuclear localization (mass spectrometry)		Nuclear +	97	5.89E-48
Tb927.6.1280	Translation initiation factor EIF-2b alpha subunit ^Δ	Cytoplasm		Gene Expression#	81	1.14E-48
Tb927.8.3820	Stress granule protein	Localization to starvation stress granules	26187993	Stress Granule#	53	2.04E-39
Tb927.3.5250	Zinc finger CCH domain-containing protein 8, ZC3H8	Cytoplasm (points)	26784394	Gene Expression#	53	2.45E-13
Tb927.9.10930	Mediator of RNA polymerase II transcription subunit 7, MED-T7	Nucleoplasm (points)	20876299	Gene Expression#	49	1.98E-18
Tb927.7.770	Ring finger domain containing protein ^Δ	Moderate nuclear lumen signal, weak cytoplasm signal		Nuclear +	47	7.14E-27
Tb927.9.7820	Hypothetical protein, conserved	Nuclear, mass spec		Nuclear○	39	3.88E-14
Tb927.1.15280	tRNA-specific adenosine deaminase, ADAT3	Cytoplasm (reticulated, weak)	17483465	Gene Expression#	37	1.59E-18
Tb927.4.1910	Hypothetical protein, conserved	Cytoplasm (points, reticulated)	26784394	Gene Expression#	35	1.10E-22
Tb927.9.15020	Hypothetical protein, conserved	Weak axoneme signal		Flagellar +	31	4.45E-20
Tb927.10.2830	Hypothetical protein, conserved	Endocytic, cytoplasm		Endocytic +	31	9.17E-31
Tb927.10.12050	LSU ribosomal protein, mitochondrial ^Δ	Kinetoplast, mitochondrion	18364347	Mitochondrial*	31	2.16E-34
Tb927.9.7200	Hypothetical protein, conserved	Kinetoplast, mitochondrion		Mitochondrial*	31	5.61E-28
Tb927.7.5460	Exosome-associated protein 3, 3' exoribonuclease, putative, EAP3	Nucleoplasm		Nuclear +	28	9.55E-27
Tb927.4.4540	Zinc finger domain, LSD1 subclass ^Δ	Cytoplasm (reticulated)		Zinc finger	25	8.84E-47
Tb927.5.4370	Hypothetical protein, conserved	Endocytic, cytoplasm		Endocytic +	24	3.59E-12
Tb927.9.7080	Hypothetical protein, conserved	Cytoplasm (patchy, points)		Mitochondrial & ER○	23	1.14E-23
Tb927.2.5210	3-Oxoacyl-ACP reductase ^Δ	Mitochondrion, kinetoplast (strong)	17166831	Mitochondrial#	23	2.16E-34
Tb927.1.12910	Phosphoglycerate mutase, iPGAM ^Δ	Mitochondrion (75%), kinetoplast (75%)		Mitochondrial*	23	6.79E-05
Tb927.1.17475	ANT1-like zinc finger-containing protein ^Δ	Cytoplasm		Zinc finger	20	1.50E-30
Tb927.9.5220	Conserved protein	Endocytic, cytoplasm (weak)		Endocytic +	19	2.60E-21
Tb927.3.4930	Hypothetical protein, conserved	Cytoplasm, flagellar cytoplasm, Nucleoplasm	9250687	Flagellar +	19	3.79E-27
Tb927.8.1930	lsl1-like splicing family	Cytoplasm (reticulated)	18951088	Gene Expression#	16	8.36E-27
Tb927.10.6850	Mitochondrial ribosomal protein S18 ^Δ	Cytoplasm (reticulated)		Mitochondrial#	16	3.68E-10
Tb927.1.1810	Ring finger domain-containing protein ^Δ	Flagellar pocket (ring)		Flagellar +	16	1.50E-18
Tb927.5.2620	Hypothetical protein, conserved	Cytoplasm (points)	24945722	Gene Expression	15	1.78E-09
Tb927.10.390	DUF2407 ubiquitin-like domain-containing protein ^Δ	Flagellum matrix proteome (BSF)	24741115	Flagellar*	14	2.78E-12
Tb927.3.1610	CMGC/CLK family protein kinase ^Δ	Nucleoplasm, cytoplasm	24453978	Kinase	14	2.82E-35
Tb927.1.12350	Hypothetical protein, conserved	Nucleus, cytoplasm (reticulated)		Nuclear +	13	2.19E-05
Tb927.8.7790	Zinc finger domain, LSD1 subclass ^Δ	Tagging not successful, ND		Mitochondrial & ER○	13	7.88E-22
Tb927.5.4150	Hypothetical protein, conserved	Paraflagellar rod		Flagellar*	13	6.29E-06
Tb927.8.3340	Hypothetical protein, conserved	Nucleoplasm		Nuclear +	13	1.28E-11
Tb927.10.1490	Temperature-dependent protein affecting M2 dsRNA replication ^Δ	Cytoplasm (weak)	20592024	Gene Expression#	12	6.62E-16
Tb927.4.890	Small nuclear ribonucleoprotein Smd3, putative, Smd3	Nucleoplasm	10900267	Gene Expression#	11	4.78E-11
Tb927.7.5360	Haemolysin-III related ^Δ	Cytoplasm		Pathogenesis	10	8.31E-27
Tb927.7.710	Heat shock 70-kDa protein, HSP70 ^Δ	Cell tip (anterior), cytoplasm, flagellar cytoplasm	30506377	Flagellar*	10	3.15E-26
Tb927.9.4930	Divalent cation transporter ^Δ	Cytoplasm (reticulated)		Trafficking	9	7.16E-54
Tb927.9.10850	Splicing factor 3B subunit 10, SF3b10 ^Δ	Nucleoplasm		Gene Expression	9	1.80E-49
Tb927.1.15600	Archaic translocase of outer membrane 14-kDa subunit, ATOM14	Mitochondrion	22267727	Gene Expression	9	9.21E-11
Tb927.10.9060	Hypothetical protein, conserved	Basal body		Mitochondrial#	8	5.86E-10
Tb927.1.1020	Leucine-rich repeat-containing protein	Hook complex		Flagellar +	8	1.61E-10
Tb927.2.2130	Small GTP-binding protein RAB6 ^Δ	Golgi apparatus		Flagellar +	8	7.70E-22

(Continued on following page)

TABLE 2 (Continued)

Gene ID	Description (TrypTag 062920)	Localization (TrypTag or proteome)	PubMed	Category	Fold change overrepresented	DESeq P-adjusted value
Tb927.1.3310	Hypothetical protein, conserved	Plasma membrane (posterior)	18242729	Glycosomal#	8	2.28E-09
Tb927.8.4200	Hypothetical protein, conserved	Cytoplasm	24945722	Gene Expression#	7	7.02E-19
Tb927.3.5190	Hypothetical protein, conserved	Mitochondrion		Mitochondrial +	7	8.48E-21
Tb927.9.3480	U5Cwc21 small nuclear ribonucleoprotein	Nucleoplasm	19429779	Gene Expression#	7	8.83E-10
Tb927.8.2391	Hypothetical protein, conserved	Not in the genome version used for tagging		ND	7	9.18E-10
Tb927.2.3780	Translation initiation factor IF-2 ^Δ	Cytoplasm		Gene Expression	6	1.12E-11
Tb927.1.1500	Conserved protein, unknown function	Cytoplasm (reticulated)	26784394	Gene Expression#	6	1.34E-05
Tb927.6.3980	Hypothetical protein, conserved	Axoneme [50%], cytoplasm		Flagellar +	6	3.88E-10

^ΔTrypTag descriptions containing the word "putative" have been replaced with ^Δ. Category data sources: +, TrypTag; ○, proteome; *, both; #, published.

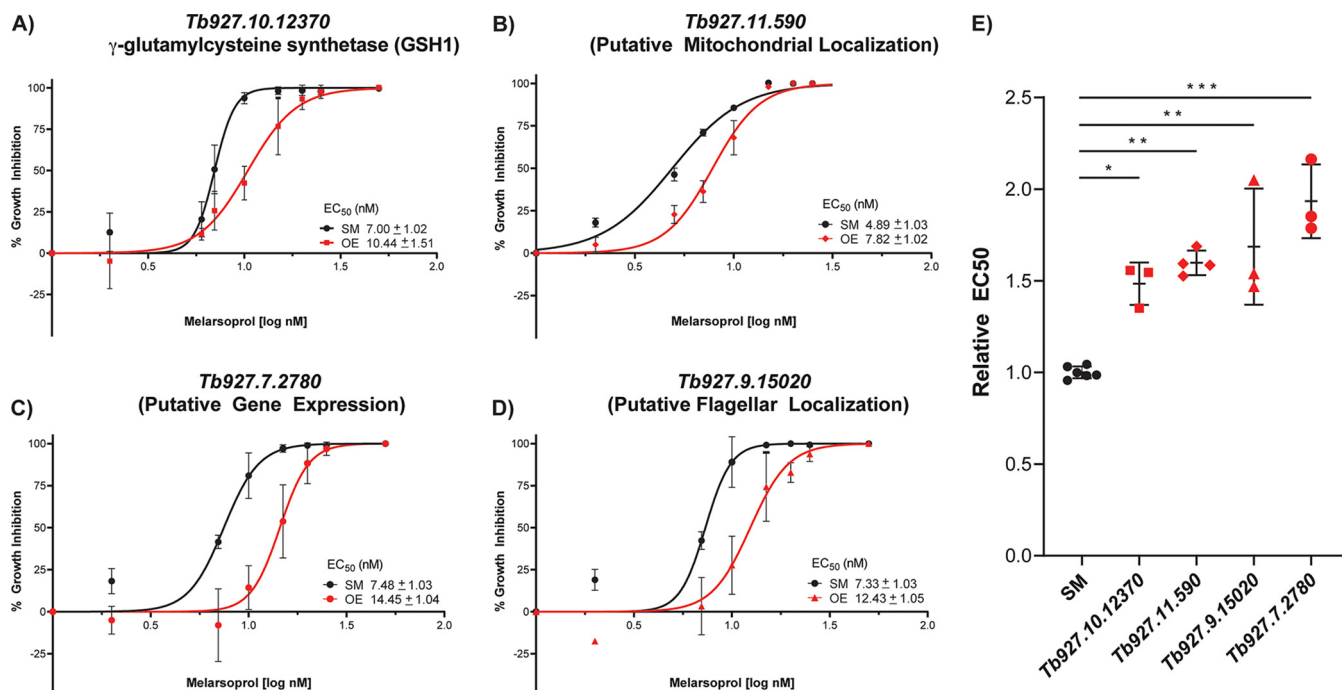


FIG 6 Melarsoprol resistance following gene overexpression. Induced expression of four hits (red lines), in comparison to those in parental cells (SM, black lines), during melarsoprol treatment with cell viability measured by alamarBlue assay to measure the resulting EC₅₀: (A) *Tb927.10.12370*. (B) *Tb927.11.590*. (C) *Tb927.7.2780*. (D) *Tb927.9.15020*. (E) Relative EC₅₀s following overexpression of each gene for at least 3 biological replicates. *P* values were derived from one-way analysis of variance (ANOVA) with Dennett's multiple-comparison test. *, *P* < 0.05; **, *P* < 0.01; ***, *P* < 0.001.

35% of trypanosomatid encoded genes largely unknown, many mysteries remain unsolved and more functional pathways must be delineated. Here, we have generated two powerful tools for forward genetic approaches: an ORFeome consisting of more than 6,500 *T. brucei* ORFs and an inducible gain-of-function library harbored in *T. brucei* parasites, whose functionality was validated in a melarsoprol proof-of-principle screen.

Once in the cell, melarsoprol is metabolized into multiple forms, including melarsen oxide, which complicates the identification of drug targets and determination of its mode of cell killing. In this study, we identified γ -glutamylcysteine synthetase (GSH1, *Tb927.10.12370*) among our top hits, whose overexpression increases the intracellular concentration of trypanothione, the primary intracellular target of melarsen oxide (26, 50, 54). It is likely that GSH1 overexpression generates sufficient levels of trypanothione [T(SH)₂] to partially overcome melarsoprol inhibition (26). Identification of GSH1 in the melarsoprol GoF screen demonstrates the ability of this tool to identify drug targets [Fig. 7, T(SH)₂ pathway] (26, 36).

Trypanothione biosynthesis and redox reactions primarily occur in the cytosol (36). Recently it was demonstrated that trypanothione and trypanothione reductase function in the mitochondrion (Fig. 7, mitochondrion in green), but these studies strongly suggested the requirement for unidentified oxidoreductases functioning in the organelle (55). Genes identified in the melarsoprol GoF screen suggest a previously uninvestigated connection between the drug and mitochondrion, though not entirely unanticipated based on trypanothione functions (36). The 10 melarsoprol GoF hits categorized as mitochondrial included β -ketoacyl-acyl carrier protein (ACP)-reductase (*Tb927.2.5210*, 23-fold overrepresented), which is required for fatty acid chain elongation in the mitochondrion as well as the production of the secondary redox carrier lipoic acid (56, 57). Here, we have also shown that overexpression of *Tb927.11.590*, which encodes a mitochondrial protein with predicted oxidoreductase and catalytic domains, can increase the EC₅₀ of melarsoprol (Fig. 6). It is intriguing to speculate that melarsoprol treatment may cause reactive oxygen species (ROS) or redox stress in the

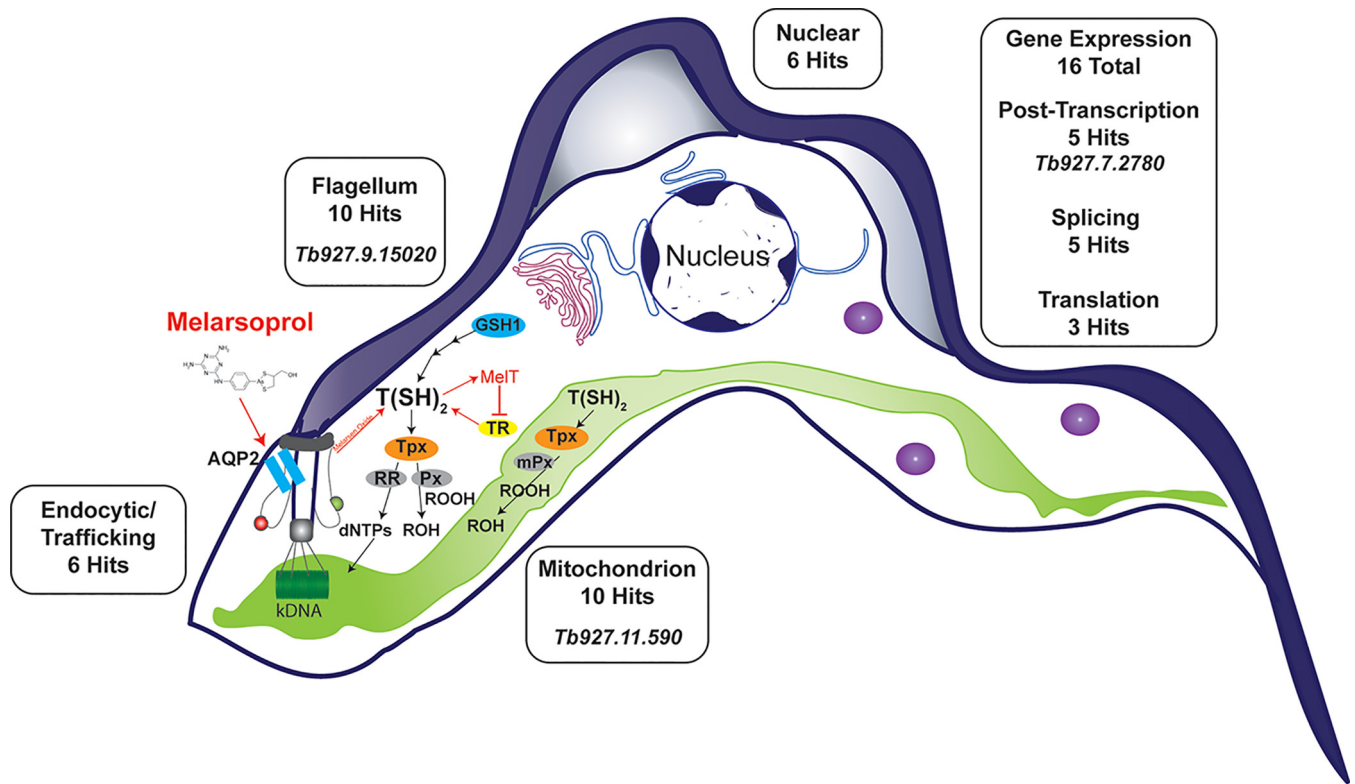


FIG 7 Categorization of GoF Hits. Hits arising from melarsoprol survival screening are shown proximal to bloodstream-form *T. brucei* cell cartoon. Rectangular boxes indicate the number of hits occurring in each major GoF screen category (see Table 2 for details). Italicized gene names in boxes are shown for genes whose induced expression promoted melarsoprol resistance (Fig. 6). The cell diagram also highlights the flagellum and flagellar pocket with the melarsoprol transporter AQP2 localized as seen in bloodstream form (34, 64). Trypanothione (T(SH)₂) biosynthesis and redox pathways are loosely depicted as follows: T(SH)₂ biosynthesis is highly simplified showing the rate-limiting enzyme GSH1, which was identified in the melarsoprol GoF screen; T(SH)₂ provides reducing equivalents to trypanothione (Tpx), which is used to reduce disulfides (not shown), peroxidases (Px), and ribonucleotide reductase (RR) for the reduction of hydroperoxides and generation of dNTPs, respectively. T(SH)₂ and Tpx are also utilized in the mitochondrion for redox reactions that include reduction of peroxidases (mPx). Melarsoprol uptake, conversion to melarsen oxide, binding with T(SH)₂ to form the stable adduct MelT, and its inhibition of trypanothione reductase (TR), which prevents the conversion of trypanothione disulfide back to T(SH)₂, are all indicated in red. Green and red spheres at the flagellar pocket indicate import and export pathways, respectively.

organelle, which might be alleviated by the overexpression of the mitochondrial proteins identified herein.

One drawback of the melarsoprol screen reported here is that we did not include a doxycycline-induced condition without melarsoprol treatment (+Dox, –Mel). Thus, any gene whose overexpression promotes survival independent of melarsoprol would be included in the hit list as a false positive. We did sequence a number of +Dox, –Mel samples over the course of the development of the library, but the results were not reproducible enough to publish, as they were performed with slightly different conditions each time. That said, we did not identify any genes as being overrepresented by >4-fold in parasites treated with Dox compared to that in untreated parasites in three separate experiments. Another caveat is that genes that code for protein products that are part of large complexes may be unstable when overexpressed individually and thus cannot be easily identified with this genetic screen.

It is unclear at this time if overrepresented genes identified in melarsoprol survivors are direct targets of melarsoprol or if they cause indirect effects that can promote resistance. Hits categorized as gene expression represent a complex list including genes associated with splicing, posttranscriptional activation, and repression. XAC1 is an established posttranscriptional activator that does not bind mRNA directly but forms complexes with other poly(A)-binding proteins (e.g., MKT1 and PBP-1) (52, 58). The gene encoding XAC1 was among the top hits, and its overexpression increased the EC₅₀ of melarsoprol (Fig. 6). While this may arise from a general increase in fitness, alterna-

tively, the overexpression of XAC1 might have a secondary effect associated with increasing the translation of enzymes required for trypanothione biosynthesis (such as GSH1 itself) or other unidentified aspects of melarsoprol cell killing.

The AQP2 transporter of melarsoprol and pentamidine is localized to the flagellar pocket in bloodstream-form parasites (Fig. 7, turquoise rectangles) (34). The large number of proteins localizing to the flagellum (10 genes) identified in melarsoprol survivors presents the intriguing possibility that they function in aspects of drug transport. For example, overexpression of accessory proteins may result in reduced drug uptake that promotes resistance. It would be useful to determine if any of these proteins affect the transport of trypanocidal drugs in a manner that might contribute to resistance. Flagellum proteins, mitochondrial proteins, and other categories of hits identified here present new testable hypotheses for future investigations that will likely uncover novel trypanosomatid biology, drug targets, and alternative mechanisms of drug resistance (Fig. 6).

The functionality of the *T. brucei* ORFeome can be extended to generate additional genetic tools, such as yeast two-hybrid libraries, tagging libraries, and dominant negative genetic screening approaches (27, 30, 31, 59). Based on the conservation of orthologous gene clusters among kinetoplastida (3), we expect the ORFeome could be used in other trypanosomatids to generate orthologous gain-of-function libraries and other tools. The vast majority of genes overrepresented in melarsoprol survivor populations (~80%) are conserved among sequenced trypanosomatid genomes. This supports the use of these tools to broadly expand our understanding of gene functions in this family of parasites. We see the GoF library as a powerful new tool that can complement existing RNAi knockdown approaches and expand our understanding of drug targets and pathways of resistance. The tools and discoveries arising from this study are expected to support broad advances in basic biology, pathogenesis, pathways of drug resistance, and the identification of the targets for compounds that selectively kill trypanosomatids.

MATERIALS AND METHODS

Methods for ORFeome generation and assessment, gain-of-function library assessment, and bioinformatic analysis of melarsoprol survivor populations are located in Text S1 in the supplemental material.

Gateway cloning and plasmids. The pENTR library was generated by cloning each size-sorted PCR product pool into pDONR221 Gateway Entry vector according to the manufacturer's specifications (Thermo Fisher Scientific, Waltham, MA) and transformed into ElectroMAX DH10B cells by electroporation (44). The resulting transformants were plated on large LB plates containing kanamycin and assessed for efficiency of transformation. Bacterial colonies were isolated from plates and grown in LB liquid cultures, which were split for maxi preps of plasmid and storage at -80°C in glycerol stocks. A *T. brucei*-specific pDEST Gateway vector, pSUN6 (Fig. S1), was generated by introducing a ccdB Gateway cassette into a pLEW type vector (46) for incorporation into the *T. brucei* genome based on rDNA spacer homology, blasticidin selection, and ORF transcription from an rRNA promoter repressed by two tetracycline operators. Pools of pENTR plasmids harboring size-sorted ORF populations were combined with pSUN6 in LR Clonase reactions and transformed into ElectroMAX DH10B cells by electroporation. The resulting transformants were plated on large LB plates containing ampicillin and assessed for efficiency of transformation; then, bacteria and DNA were isolated as described above for pENTR steps. The resulting plasmid libraries of pENTR and pTrypLib ORFeome Gateway cloning steps were assessed by NGS (Text S1). Following the initial assessment of "missing" ORFs from both pENTR and pTrypLib cloning libraries, "missing" PCR products were isolated from original plates, using a Perkin-Emer Janus Automated Workstation, to generate 8 new pools of size-sorted PCRs (Table S2), which underwent the same series of Gateway cloning reactions described above and subjected to NGS analysis. The final NGS-validated pTrypLib library plasmids were pooled to generate a single pTrypLib ORFeome for introduction into the *T. brucei* genome.

***T. brucei* cell lines, transfections, and GoF parasite library generation.** Cell lines were generated from Lister 427 bloodstream-form trypanosomes derived from the "single marker" (SM) line (60) and maintained in HMI-9 medium (61) under appropriate drug selection when indicated. A landing pad (LP) cell line was generated using plasmids gifted to us by the Alford Lab and validated for inducible gene expression, prior to transfection with pRPaSc^{*} as described previously (6, 62). LP parasites harboring the I-SceI cut site and I-SceI endonuclease gene targeted at an rDNA spacer were doxycycline induced to permit I-SceI cutting prior to pTrypLib ORFeome transfection by AMAXA Nucleofector (63). To generate the *T. brucei* GoF library described here, four 100-ml flask cultures grown to ~1 million cells/ml were AMAXA transfected with 10 μg pTrypLib DNA in four separate transfection reaction mixtures, which were then pooled into a single cell population in 500 ml of HMI-9 and recovered in a large roller flask, to which blasticidin was added 12 h posttransfection (Fig. 3C). An additional four transfections were completed in

parallel with Tris-EDTA (TE; mock) to compare outgrowth with GoF library transfection. The resulting blasticidin-recovered GoF library population was expanded to an 800-ml culture at ~1 million cells per ml and saved in aliquots of ~25 million cells per vial for future genetic screens. Cells were also sampled prior to freezing for NGS analysis (GoF library, described below) and after freeze-thaw (GoF_L1).

Single-gene overexpression cell lines were generated by cloning ORFs of interest into pLEW100v5-BSD (plasmid 27658; Addgene, Watertown, MA), which, following validation, were digested with NotI and transfected into SM cells by AMAXA.

Quantitative PCR assessment of ORF induction. Individual cloned ORFs were selected randomly from pTrypLib colonies plated on LB originating from the pool “2_known,” ORFs confirmed by traditional DNA sequencing and DNAs arising from 4 individual ORF-harboring pTrypLib vectors were transfected into LP-harboring pRPaSc* by AMAXA as described above. This generated a “low-complexity library” following transfection and recovery, which was split into no Dox and +Dox conditions for 24 h; RNA was extracted and cDNA was prepared with Superscript III (18080044; Thermo Fisher) prior to qPCR analysis. Quantitative PCR data were produced on a Bio-Rad CFX96 real-time PCR detection system with iTaq Universal SYBR green Supermix (1725121; Bio-Rad). The forward primer anneals to the *attB1* site (5'-GGGGACAAGTTTGTACAAAAAAGCAGGCT) and reverse primers were unique to each ORF: *Tb927.8.2230* (primer, 5'-CACGGTTTTGCCCATTCGT), *Tb927.1.4830* (primer, 5'-ATTTTTGCCGAAGCGCTTGA), *Tb927.10.12940* (primer, 5'-CCGTGATCCCTGTGACAT), and *Tb927.11.15810* (primer, 5'-CACCACCCGATGTACGGTAG). Because the forward primer anneals to the *attB1* site present only in the pTrypLib backbone, only those mRNAs arising from the exogenous ORFs integrated at the rDNA spacer, rather than the endogenous ORF, can be detected. Fold changes in transcripts level with Dox and without Dox were plotted (Fig. 3B).

Melarsoprol GoF library screening. GoF library cells were seeded for each condition at 1×10^5 cell/ml, induced with doxycycline (1 μ g/ml) for 24 h (for induced cultures, +Dox) (Fig. 4), and grown in HMI-9 medium containing Dox (when appropriate) plus melarsoprol at 17 nM or 35 nM (BoC Sciences, CAS 494-79-1). Melarsoprol stocks were diluted in dimethyl sulfoxide (DMSO), and cultures were treated for the duration indicated in the figures and text (Fig. 4C, bottom, time bar indicates time points of replenishment of melarsoprol and/or Dox and time points of sample harvest). GoF library-harboring cells were thawed from a single starting vial of approximately 25 million cells, propagated for 3 days prior to day -1 Dox induction, and on day 0, were split into 100-ml biological triplicates for untreated GoF_L (GoF_L, no Dox), uninduced (no Dox), and induced (+Dox) samples. Two elongation times were employed during PCR enrichment, GoF_L1 for 75 s and GoF_L2 for 20 s, to determine if amplification time resulted in a sequencing bias. Sequencing data were obtained in biological triplicates from GoF_L1 and GoF_L2 libraries (no melarsoprol treatment) and the two sets of melarsoprol-selected parasites (MEL1 and MEL2, NGS libraries were generated using 20-s elongation time). GoF library-harboring cells were recovered from each replicate and condition (GoF_L, MEL, and MEL), and genomic DNA was fragmented and prepared for ORFeome-specific Illumina sequencing (Fig. S3).

EC₅₀ determination by alamarBlue. For EC₅₀ determination, induced and uninduced cells were plated across a melarsoprol dilution series, and viability was assessed after 72 h using alamarBlue (Thermo Fisher) as previously described (11). All experiments were performed in biological triplicates.

SUPPLEMENTAL MATERIAL

Supplemental material is available online only.

TEXT S1, PDF file, 0.1 MB.

FIG S1, PDF file, 0.5 MB.

FIG S2, PDF file, 2.1 MB.

FIG S3, PDF file, 3.1 MB.

FIG S4, PDF file, 3.4 MB.

TABLE S1, PDF file, 1.2 MB.

TABLE S2, PDF file, 0.4 MB.

DATA SET S1, XLSX file, 0.9 MB

DATA SET S2, XLSX file, 2.6 MB.

DATA SET S3, XLSX file, 0.1 MB.

ACKNOWLEDGMENTS

We thank the individuals and consortiums whose support made this work possible. Marilyn Parsons (now of Seattle Children's Hospital) provided prepublication access to the TREU927 ribosomal profiling data that provided the gene starts and stops for all ORFeome-targeted ORFs. Christine Clayton and Esteban Erben (Heidelberg University) provided their essential insights into methods for successful ORFeome Gateway cloning. Data provided directly from the TrypTag.org consortium was critical in the categorization of hits arising from melarsoprol GoF screening. Similarly, TritypDB.org was an essential resource throughout all stages of the work described herein. We also thank F. Nina Papavasiliou, whose support and generosity have been invaluable.

REFERENCES

- Alcántara LM, Ferreira TCS, Gadelha FR, Miguel DC. 2018. Challenges in drug discovery targeting TriTryp diseases with an emphasis on leishmaniasis. *Int J Parasitol Drug Resist* 8:430–439. <https://doi.org/10.1016/j.ijpddr.2018.09.006>.
- Fairlamb AH, Gow NAR, Matthews KR, Waters AP. 2016. Drug resistance in eukaryotic microorganisms. *Nat Microbiol* 1:16092. <https://doi.org/10.1038/nmicrobiol.2016.92>.
- El-Sayed NM, Myler PJ, Blandin G, Berriman M, Crabtree J, Aggarwal G, Caler E, Renauld H, Worthey EA, Hertz-Fowler C, Ghedin E, Peacock C, Bartholomeu DC, Haas BJ, Tran A-N, Wortman JR, Alsmark UCM, Angiuoli S, Anupama A, Badger J, Bringaud F, Cadag E, Carlton JM, Cerqueira GC, Creasy T, Delcher AL, Djikeng A, Embley TM, Hauser C, Ivens AC, Kummerfeld SK, Pereira-Leal JB, Nilsson D, Peterson J, Salzberg SL, Shallom J, Silva JC, Sundaram J, Westenberger S, White O, Melville SE, Donelson JE, Andersson B, Stuart KD, Hall N. 2005. Comparative genomics of trypanosomatid parasitic protozoa. *Science* 309:404–409. <https://doi.org/10.1126/science.1112181>.
- Alsford S, Kelly JM, Baker N, Horn D. 2013. Genetic dissection of drug resistance in trypanosomes. *Parasitology* 140:1478–1491. <https://doi.org/10.1017/S003118201300022X>.
- Currier RB, Cooper A, Burrell-Saward H, MacLeod A, Alsford S. 2018. Decoding the network of *Trypanosoma brucei* proteins that determines sensitivity to apolipoprotein-L1. *PLoS Pathog* 14:e1006855. <https://doi.org/10.1371/journal.ppat.1006855>.
- Glover L, Alsford S, Baker N, Turner DJ, Sanchez-Flores A, Hutchinson S, Hertz-Fowler C, Berriman M, Horn D. 2015. Genome-scale RNAi screens for high-throughput phenotyping in bloodstream-form African trypanosomes. *Nat Protoc* 10:106–133. <https://doi.org/10.1038/nprot.2015.005>.
- Jones NG, Thomas EB, Brown E, Dickens NJ, Hammarton TC, Mottram JC. 2014. Regulators of *Trypanosoma brucei* cell cycle progression and differentiation identified using a kinome-wide RNAi screen. *PLoS Pathog* 10:e1003886. <https://doi.org/10.1371/journal.ppat.1003886>.
- Mony BM, MacGregor P, Ivens A, Rojas F, Cowton A, Young J, Horn D, Matthews K. 2014. Genome-wide dissection of the quorum sensing signalling pathway in *Trypanosoma brucei*. *Nature* 505:681–685. <https://doi.org/10.1038/nature12864>.
- Rico E, Ivens A, Glover L, Horn D, Matthews KR. 2017. Genome-wide RNAi selection identifies a regulator of transmission stage-enriched gene families and cell-type differentiation in *Trypanosoma brucei*. *PLoS Pathog* 13:e1006279. <https://doi.org/10.1371/journal.ppat.1006279>.
- Alsford S, Eckert S, Baker N, Glover L, Sanchez-Flores A, Leung KF, Turner DJ, Field MC, Berriman M, Horn D. 2012. High-throughput decoding of antitrypanosomal drug efficacy and resistance. *Nature* 482:232–236. <https://doi.org/10.1038/nature10771>.
- Baker N, Alsford S, Horn D. 2011. Genome-wide RNAi screens in African trypanosomes identify the nifurtimox activator NTR and the eiforinithine transporter AAT6. *Mol Biochem Parasitol* 176:55–57. <https://doi.org/10.1016/j.molbiopara.2010.11.010>.
- Zhang N, Zoltner M, Leung K-F, Scullion P, Hutchinson S, del Pino RC, Vincent IM, Zhang Y-K, Freund YR, Alley MRK, Jacobs RT, Read KD, Barrett MP, Horn D, Field MC. 2018. Host-parasite co-metabolic activation of antitrypanosomal aminomethyl-benzoxaboroles. *PLoS Pathog* 14:e1006850. <https://doi.org/10.1371/journal.ppat.1006850>.
- Normark S, Edlund T, Grundström T, Bergström S, Wolf-Watz H. 1977. *Escherichia coli* K-12 mutants hyperproducing chromosomal beta-lactamase by gene repetitions. *J Bacteriol* 132:912–922. <https://doi.org/10.1128/JB.132.3.912-922.1977>.
- Rine J, Hansen W, Hardeman E, Davis RW. 1983. Targeted selection of recombinant clones through gene dosage effects. *Proc Natl Acad Sci U S A* 80:6750–6754. <https://doi.org/10.1073/pnas.80.22.6750>.
- Sandegren L, Andersson DI. 2009. Bacterial gene amplification: implications for the evolution of antibiotic resistance. *Nat Rev Microbiol* 7:578–588. <https://doi.org/10.1038/nrmicro2174>.
- Rao SPS, Barrett MP, Dranoff G, Faraday CJ, Gimpelewicz CR, Hailu A, Jones CL, Kelly JM, Lazdins-Helds JK, Mäser P, Mengel J, Mottram JC, Mowbray CE, Sacks DL, Scott P, Späth GF, Tarleton RL, Spector JM, Diagona TT. 2019. Drug discovery for kinetoplastid diseases: future directions. *ACS Infect Dis* 5:152–157. <https://doi.org/10.1021/acinfecdis.8b00298>.
- Gabriel HB, Azevedo MF, Kimura EA, Katzin AM. 2018. *Plasmodium falciparum* parasites overexpressing farnesyl diphosphate synthase/geranylgeranyl diphosphate synthase are more resistant to risperidone. *Mem Inst Oswaldo Cruz* 113:e180174. <https://doi.org/10.1590/0074-02760180174>.
- Gambini L, Rizzi L, Pedretti A, Tagliatalata-Scafati O, Carucci M, Pancotti A, Galli C, Read M, Giuriso E, Romeo S, Russo I. 2015. Picomolar inhibition of plasmepsin V, an essential malaria protease, achieved exploiting the prime region. *PLoS One* 10:e0142509. <https://doi.org/10.1371/journal.pone.0142509>.
- Prelich G. 2012. Gene overexpression: uses, mechanisms, and interpretation. *Genetics* 190:841–854. <https://doi.org/10.1534/genetics.111.136911>.
- Clayton C. 2016. Gene expression in kinetoplastids. *Curr Opin Microbiol* 32:46–51. <https://doi.org/10.1016/j.mib.2016.04.018>.
- Begolo D, Erben E, Clayton C. 2014. Drug target identification using a trypanosome overexpression library. *Antimicrob Agents Chemother* 58:6260–6264. <https://doi.org/10.1128/AAC.03338-14>.
- Wall RJ, Rico E, Lukac I, Zuccotto F, Elg S, Gilbert IH, Freund Y, Alley MRK, Field MC, Wyllie S, Horn D. 2018. Clinical and veterinary trypanocidal benzoxaboroles target CPSF3. *Proc Natl Acad Sci U S A* 115:9616–9621. <https://doi.org/10.1073/pnas.1807915115>.
- Erben ED, Fadda A, Lueong S, Hoheisel JD, Clayton C. 2014. A genome-wide tethering screen reveals novel potential post-transcriptional regulators in *Trypanosoma brucei*. *PLoS Pathog* 10:e1004178. <https://doi.org/10.1371/journal.ppat.1004178>.
- Lueong S, Merce C, Fischer B, Hoheisel JD, Erben ED. 2016. Gene expression regulatory networks in *Trypanosoma brucei*: insights into the role of the mRNA-binding proteome. *Mol Microbiol* 100:457–471. <https://doi.org/10.1111/mmi.13328>.
- Singh A, Minia I, Droll D, Fadda A, Clayton C, Erben E. 2014. Trypanosome MKT1 and the RNA-binding protein ZC3H1: interactions and potential roles in post-transcriptional regulatory networks. *Nucleic Acids Res* 42:4652–4668. <https://doi.org/10.1093/nar/gkt1416>.
- Shahi SK, Krauth-Siegel RL, Clayton CE. 2002. Overexpression of the putative thiol conjugate transporter TbMRPA causes melarsoprol resistance in *Trypanosoma brucei*. *Mol Microbiol* 43:1129–1138. <https://doi.org/10.1046/j.1365-2958.2002.02831.x>.
- Rual J-F, Hill DE, Vidal M. 2004. ORFeome projects: gateway between genomics and omics. *Curr Opin Chem Biol* 8:20–25. <https://doi.org/10.1016/j.cbpa.2003.12.002>.
- Li Q-R, Carvunis A-R, Yu H, Han J-DJ, Zhong Q, Simonis N, Tam S, Hao T, Klitgord NJ, Dupuy D, Mou D, Wapinski I, Reggev A, Hill DE, Cusick ME, Vidal M. 2008. Revisiting the *Saccharomyces cerevisiae* predicted ORFeome. *Genome Res* 18:1294–1303. <https://doi.org/10.1101/gr.076661.108>.
- Gallegos ME, Balakrishnan S, Chandramouli P, Arora S, Azameera A, Babushekar A, Bargoma E, Bokhari A, Chava SK, Das P, Desai M, Decena D, Saramma SDD, Dey B, Doss A-L, Gor N, Gudiputi L, Guo C, Hande S, Jensen M, Jones S, Jones N, Jorgens D, Karamchedu P, Kamrani K, Kolora LD, Kristensen L, Kwan K, Lau H, Maharaj P, Mander N, Mangipudi K, Menakuru H, Mody V, Mohanty S, Mukkamala S, Mundra SA, Nagaraju S, Narayanaswamy R, Ndungu-Case C, Noorbakhsh M, Patel J, Patel P, Pendem SV, Ponakala A, Rath M, Robles MC, Rokkam D, Roth C, Sasidharan P, et al. 2012. The *C. elegans* Rab family: identification, classification and toolkit construction. *PLoS One* 7:e49387. <https://doi.org/10.1371/journal.pone.0049387>.
- Mehla J, Caufield JH, Uetz P. 2015. The yeast two-hybrid system: a tool for mapping protein–protein interactions. *Cold Spring Harb Protoc* 2015:top083345. <https://doi.org/10.1101/pdb.top083345>.
- Bischof J, Duffraisse M, Furger E, Ajuria L, Giraud G, Vanderperre S, Paul R, Björklund M, Ahr D, Ahmed AW, Spinelli L, Brun C, Basler K, Merabet S. 2018. Generation of a versatile BiFC ORFeome library for analyzing protein-protein interactions in live *Drosophila*. *Elife* 7:e38853. <https://doi.org/10.7554/eLife.38853>.
- King J, Foster J, Davison JM, Rawls JF, Breton G. 2018. Zebrafish transcription factor ORFeome for gene discovery and regulatory network elucidation. *Zebrafish* 15:202–205. <https://doi.org/10.1089/zeb.2017.1486>.
- Fairlamb AH, Horn D. 2018. Melarsoprol resistance in African trypanosomiasis. *Trends Parasitol* 34:481–492. <https://doi.org/10.1016/j.pt.2018.04.002>.
- Baker N, de Koning HP, Mäser P, Horn D. 2013. Drug resistance in African

- trypanosomiasis: the melarsoprol and pentamidine story. Trends Parasitol 29:110–118. <https://doi.org/10.1016/j.pt.2012.12.005>.
35. Deeks ED. 2019. Fexinidazole: first global approval. Drugs 79:215–220. <https://doi.org/10.1007/s40265-019-1051-6>.
 36. Krauth-Siegel RL, Comini MA. 2008. Redox control in trypanosomatids, parasitic protozoa with trypanothione-based thiol metabolism. Biochim Biophys Acta 1780:1236–1248. <https://doi.org/10.1016/j.bbagen.2008.03.006>.
 37. Fairlamb AH, Henderson GB, Cerami A. 1989. Trypanothione is the primary target for arsenical drugs against African trypanosomes. Proc Natl Acad Sci U S A 86:2607–2611. <https://doi.org/10.1073/pnas.86.8.2607>.
 38. Agnihotri P, Singh SP, Shakya AK, Pratap JV. 2016. Biochemical and biophysical characterization of Leishmania donovani gamma-glutamylcysteine synthetase. Biochem Biophys Rep 8:127–138. <https://doi.org/10.1016/j.bbrep.2016.08.016>.
 39. Richardson JL, Nett IRE, Jones DC, Abdille MH, Gilbert IH, Fairlamb AH. 2009. Improved tricyclic inhibitors of trypanothione reductase by screening and chemical synthesis. Chemmedchem 4:1333–1340. <https://doi.org/10.1002/cmdc.200900097>.
 40. Eqbal A, Suman SS, Anwar S, Singh KP, Zaidi A, Sardar AH, Das P, Ali V. 2014. Stage-dependent expression and up-regulation of trypanothione synthetase in amphotericin B resistant Leishmania donovani. PLoS One 9:e97600. <https://doi.org/10.1371/journal.pone.0097600>.
 41. Vickers TJ, Fairlamb AH. 2004. Trypanothione S-transferase activity in a trypanosomatid ribosomal elongation factor 1B. J Biol Chem 279:27246–27256. <https://doi.org/10.1074/jbc.M311039200>.
 42. González-Chávez Z, Vázquez C, Mejía-Tlachi M, Márquez-Dueñas C, Manning-Cela R, Encalada R, Rodríguez-Enríquez S, Michels PAM, Moreno-Sánchez R, Saavedra E. 2019. Gamma-glutamylcysteine synthetase and tryparedoxin 1 exert high control on the antioxidant system in Trypanosoma cruzi contributing to drug resistance and infectivity. Redox Biol 26:101231. <https://doi.org/10.1016/j.redox.2019.101231>.
 43. Parsons M, Ramasamy G, Vasconcelos EJR, Jensen BC, Myler PJ. 2015. Advancing Trypanosoma brucei genome annotation through ribosome profiling and spliced leader mapping. Mol Biochem Parasitol 202:1–10. <https://doi.org/10.1016/j.molbiopara.2015.09.002>.
 44. Katzen F. 2007. Gateway recombinational cloning: a biological operating system. Expert Opin Drug Discov 2:571–589. <https://doi.org/10.1517/17460441.2.4.571>.
 45. Adey A, Morrison HG, Asan, Xun X, Kitzman JO, Turner EH, Stackhouse B, MacKenzie AP, Caruccio NC, Zhang X, Shendure J. 2010. Rapid, low-input, low-bias construction of shotgun fragment libraries by high-density in vitro transposition. Genome Biol 11:R119. <https://doi.org/10.1186/gb-2010-11-12-r119>.
 46. Siegel TN, Tan KSW, Cross GAM. 2005. Systematic study of sequence motifs for RNA trans splicing in Trypanosoma brucei. Mol Cell Biol 25:9586–9594. <https://doi.org/10.1128/MCB.25.21.9586-9594.2005>.
 47. Dean S, Sunter JD, Wheeler RJ. 2017. TrypTag.org: a trypanosome genome-wide protein localisation resource. Trends Parasitol 33:80–82. <https://doi.org/10.1016/j.pt.2016.10.009>.
 48. Dean S, Sunter J, Wheeler RJ, Hodgkinson I, Gluenz E, Gull K. 2015. A toolkit enabling efficient, scalable and reproducible gene tagging in trypanosomatids. Open Biol 5:140197. <https://doi.org/10.1098/rsob.140197>.
 49. Ziková A, Verner Z, Nenarokova A, Michels PAM, Lukeš J. 2017. A paradigm shift: the mitoproteomes of procyclic and bloodstream Trypanosoma brucei are comparably complex. PLoS Pathog 13:e1006679. <https://doi.org/10.1371/journal.ppat.1006679>.
 50. Lueder DV, Phillips MA. 1996. Characterization of Trypanosoma brucei γ -glutamylcysteine synthetase, an essential enzyme in the biosynthesis of trypanothione (diglutathionylspermidine). J Biol Chem 271:17485–17490. <https://doi.org/10.1074/jbc.271.29.17485>.
 51. Fonseca MS, Comini MA, Resende BV, Santi AMM, Zoboli AP, Moreira DS, Murta SMF. 2017. Ornithine decarboxylase or gamma-glutamylcysteine synthetase overexpression protects Leishmania (Vianna) guyanensis against antimony. Exp Parasitol 175:36–43. <https://doi.org/10.1016/j.exppara.2017.02.001>.
 52. do Nascimento LM, Terrao M, Marucha KK, Liu B, Egler F, Clayton C. 2020. The RNA-associated proteins MKT1 and MKT1L form alternative PBP1-containing complexes in Trypanosoma brucei. J Biol Chem 295:10940–10955. <https://doi.org/10.1074/jbc.RA120.013306>.
 53. Matthews KR. 2015. 25 years of African trypanosome research: from description to molecular dissection and new drug discovery. Mol Biochem Parasitol 200:30–40. <https://doi.org/10.1016/j.molbiopara.2015.01.006>.
 54. Fairlamb AH, Cerami A. 1992. Metabolism and functions of trypanothione in the Kinetoplastida. Annu Rev Microbiol 46:695–729. <https://doi.org/10.1146/annurev.mi.46.100192.003403>.
 55. Ebersoll S, Bogacz M, Günter LM, Dick TP, Krauth-Siegel RL. 2020. A tryparedoxin-coupled biosensor reveals a mitochondrial trypanothione metabolism in trypanosomes. Elife 9:e53227. <https://doi.org/10.7554/eLife.53227>.
 56. Stephens JL, Lee SH, Paul KS, Englund PT. 2007. Mitochondrial fatty acid synthesis in Trypanosoma brucei. J Biol Chem 282:4427–4436. <https://doi.org/10.1074/jbc.M609037200>.
 57. Solmonson A, DeBerardinis RJ. 2018. Lipoic acid metabolism and mitochondrial redox regulation. J Biol Chem 293:7522–7530. <https://doi.org/10.1074/jbc.TM117.000259>.
 58. Nascimento L, Terrao M, Marucha KK, Liu B, Egler F, Clayton C. 3 March 2020. Essential PBP1-associated proteins of Trypanosoma brucei. BioRxiv <https://doi.org/10.1101/2020.03.02.973057>.
 59. Grant IM, Balcha D, Hao T, Shen Y, Trivedi P, Patrushev I, Fortriede JD, Karpinka JB, Liu L, Zorn AM, Stukenberg PT, Hill DE, Gilchrist MJ. 2015. The Xenopus ORFeome: a resource that enables functional genomics. Dev Biol 408:345–357. <https://doi.org/10.1016/j.ydbio.2015.09.004>.
 60. Wirtz E, Leal S, Ochatt C, Cross GM. 1999. A tightly regulated inducible expression system for conditional gene knock-outs and dominant-negative genetics in Trypanosoma brucei. Mol Biochem Parasitol 99:89–101. [https://doi.org/10.1016/S0166-6851\(99\)00002-X](https://doi.org/10.1016/S0166-6851(99)00002-X).
 61. Hirumi H, Hirumi K. 1994. Axenic culture of African trypanosome bloodstream forms. Parasitol Today 10:80–84. [https://doi.org/10.1016/0169-4758\(94\)90402-2](https://doi.org/10.1016/0169-4758(94)90402-2).
 62. Alsford S, Kawahara T, Glover L, Horn D. 2005. Tagging a T. brucei RRNA locus improves stable transfection efficiency and circumvents inducible expression position effects. Mol Biochem Parasitol 144:142–148. <https://doi.org/10.1016/j.molbiopara.2005.08.009>.
 63. Burkard G, Fragoso CM, Roditi I. 2007. Highly efficient stable transformation of bloodstream forms of Trypanosoma brucei. Mol Biochem Parasitol 153:220–223. <https://doi.org/10.1016/j.molbiopara.2007.02.008>.
 64. Baker N, Glover L, Munday JC, Andrés DA, Barrett MP, de Koning HP, Horn D. 2012. Aquaglyceroporin 2 controls susceptibility to melarsoprol and pentamidine in African trypanosomes. Proc Natl Acad Sci U S A 109:10996–11001. <https://doi.org/10.1073/pnas.1202885109>.